PREPARATION OF REDUCED GRAPHENE OXIDE NANOPARTICLES AND ITS USE IN TREATMENT OF TUMOUR BEARING MICE

Mostafa Yahia Mostafa[2] Mahmoud S. Elbasiouny[1], Tarek Atta[2], Tarek F. Elwakil[1], Hesham Ramzy Tantawy[2]

ABSTRACT:

Nano-sized reduced graphene oxide (RGO) shows potential for biomedical uses such as photothermal therapy of cancer. It is discovered the novel property of RGO nanoparticles, which release a significant amount of heat by the stimulation with near infrared leaser. This phenomenon supports the hypothesis thermal cytotoxicity of cancer cells by the induced leaser stimulated heat. The synthesis of RGO from commercial graphite procurer was carried out using improved hummer method followed by green reduction with ascorbic acid. Morphological characterization carried out via scanning electron microscopy (SEM) and transmission electron microscopy (TEM) demonstrated the successful exfoliation of graphite procurer to RGO. Furthermore, Raman spectrum of RGO exhibited G band at 1582 cm^{-1} (typical also for graphite), and broad D band (characteristic for RGO) appears at 1350 cm^{-1}; this characteristic peak confirmed the successful formation of RGO. Tumor bearing mice were divided into four groups three served as positive and negative control groups the treated group injected by RGO and irradiated by 980nm laser. The assessment of tumor response showed marked response of tumor to hyperthermia produced by RGO stimulated heat induced by near infrared laser.

KEY WORDS: nanoparticles, reduced graphene oxide, hyperthermia, tumor bearing mice, near infrared laser.

1 Department of medical applications of lasers, national institute of laser enhanced science, Cairo University.
2 Military Technical Collage (MTC), Cairo, Egypt.

Introduction

Cancer has one of the highest worldwide mortality indices of any disease. Treatment includes chemotherapy, radiotherapy, and immunotherapy but despite the efforts and efficacy of these strategies mortality rates are still very high [1, 2]. Most anticancer drugs and radiotherapy cause the death of sensitive cells by inducing apoptosis [3].

Resistance is one of the major limitations in chemotherapy. Therefore, the search for new strategies and/or compounds with antitumoral properties that may increase the efficacy of the current chemotherapeutic agents is of great interest [7–9]. Hyperthermia is a promising alternative for cancer treatment that is based on increasing the temperature (40–43C) specifically in tumor tissue and the therapeutic effect depends on the strength and treatment duration [10].

A large number of experimental studies have also reported that hyperthermia increases the effectiveness of conventional antineoplastic therapies [11–13]. It is known that the architecture of the vasculature in solid tumor tissues is complex, with a hypoxic and acidic microenvironment [14]. In this scenario, cancer cells are highly sensitive to hyperthermia treatment and most of the healthy cells around tumor tissues are not damaged [15]. Hyperthermia induces the unfolding and aggregation of proteins, damage of the cell membrane, and disruption of cell cytoskeleton [16].

Although this treatment has shown low toxicity, mild side effects, effectiveness in killing cancer cells and apoptosis inducing properties, the acquisition of thermo tolerance is a main clinical problem [17].

Based on these positive clinical trials, hyperthermia and thermal ablation are recognized in clinical oncology for a number of tumor indications. Hyperthermia is routinely used for locally advanced cervical cancer patients unfit for chemotherapy, for recurrent breast cancer, non-muscle invasive bladder cancer and soft tissue sarcoma. Thermal ablation is currently in routine clinical use for a large number of indications, including hepatocellular carcinoma, renal cell carcinoma (the most common type of kidney cancer), primary and secondary lung tumors, prostate cancer, non-surgical liver metastases and adrenal metastases.

The realization of good clinical results requires high quality heating equipment, and thus a significant amount of research has been undertaken

This has been generally associated with the synthesis and accumulation of pro-survival heat shock proteins, especially HSP70, among other factors [18]. Hyperthermia treatments aim to induce relatively mild tumor heating up to a maximum temperature of 45°C. The therapeutic effect depends on the temperature and the duration of heating (thermal dose) [2–4].

Thermal ablation aims at generation of temperatures over 50°C for a few minutes in a single session to destroy tumor cells by heat alone. These excessive temperatures cause very rapid cell death by coagulation and protein denaturation, leading to both necrosis and apoptosis, depending on the dose. As explained in the previous paragraph, Arrhenius relationships can also be applied to thermal ablation to predict thermal damage and physical changes associated with thermal exposure in several tissue types [16].

Depending on the mode of energy delivery, thermal ablation can be used as a minimally invasive alternative to surgical resection. However, in the tumor periphery beyond the border of immediate tissue coagulation, non-lethal, but hyperthermic temperatures are achieved and therefore the combination of thermal ablation with chemotherapy, radiotherapy, or immunotherapy, is also attracting growing clinical interest for effectively treating both the tumor and its periphery [17–19].

Over the past several decades increasing knowledge gained about the mechanisms of action of both hyperthermia and thermal ablation have had positive effects on treatment outcome in several randomized clinical trials for both hyperthermia and thermal ablation [21].

Materials & Chemicals

The chemicals used in the experimental work are in the reagent grade. They were obtained from the indicated sources, with some specified purities, with no further purification, as shown in **table (1).**

Table (1). The chemical used in preparation

Chemicals	Purity	Source
Graphite	99.5%	NICE / India
Potassium Permanganate	98%	Alpha Chemicals/ India
Sulfuric Acid	98%	Alpha Chemicals/ India
Phosphoric Acid	85%	Alpha Chemicals/ India
Hydrochloric Acid	36%	Alpha Chemicals/ India
Hydrogen Peroxide	35%	Alpha Chemicals/ India
Ascorbic Acid	98%	Alpha Chemicals/ India
Ethanol	99%	Alpha Chemicals/ India

Preparation of reduced graphene oxide (RGO)

Chemical oxidation and exfoliation of the graphite precursor was carried out via improved hummer method in such similar approach as illustrated in pervious reference [1-3]. Typically, 5g of graphite powder was added to 600 ml concentrated sulfuric acid H_2SO_4 and 75ml of concentrated phosphoric acid H_3PO_4 in a 2 L beaker kept at room temperature. Afterwards, 30g of potassium permanganate $KMnO_4$ was gradually added to the mixture stepwise with contentious stirring for 1 hour. Further, the final obtained mixture was kept under stirring under at room temperature for 24 hours. Later, the obtained dense mixture was added in portions to 4L of cold distilled water in 5L beaker, which kept at 2 C^0 in water path for under continuous stirring. Subsequently, the yellowish colour of the successful graphene oxide (GO) product was observed as 100ml of 15% hydrogen peroxide was added to the ending diluted mixture. The product was left for decantation and washed three times with acidified water (1M HCl), followed by distilled water three times for neutralization. Regarding the reduction step, the obtained washed GO was transferred to 2L beaker and the reduction process was carried out by employing 10g of ascorbic acid as reducing agent. It was added stepwise to the GO dispersion under vigorous mixing at 80 C^0 then the mixture was left for 24 hr. Synthesis drill for RGO is shown in figure 1. Finally, the obtained black reduced graphene oxide (RGO) product was washed with distilled water by decantation three times before vacuum filtration. The obtained RGO was separated and washed via vacuum filtration with distilled water followed by ethanol remove any remnant by-products or impurities. At the end the isolated fluffy RGO powder was dried at room temperature for 24h followed by drying in oven at 40 C^0 for 24hr.
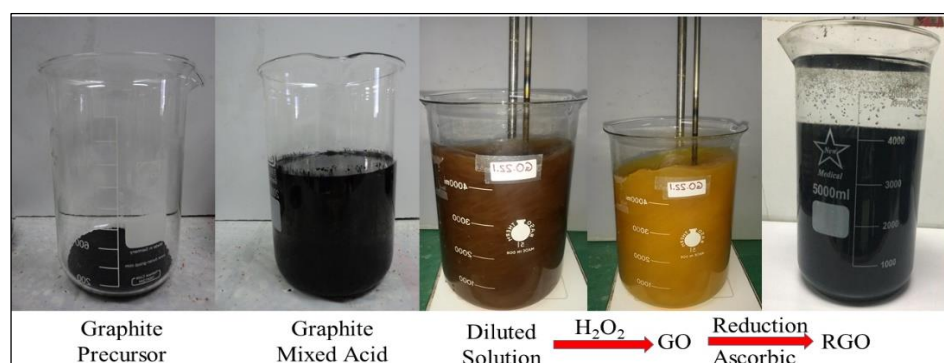

Figure (1): Synthesis drill for RGO

Instrumentations and Characterization

The morphology of starting graphite particles was investigated using SEM (EVO-MA10, ZEISS). While, morphology of synthesized RGO particles was visualized with TEM (JEM-2100F, JEOL, Japan). Furthermore, the crystalline structure was investigated using XRD (XRD, D8 Advance, Bruker Corporation, Germany). Moreover, Raman spectroscopic measurements was performed on RGO powder sample by using a dispersive Raman microscope (model Senterra II, Bruker, Germany). Spectroscopic analysis was performed on Raman spectra were continuously collected with spectral resolution $4cm^{-1}$. A Nikon 20× objective used to focus the Raman excitation source (10 mW, 532nm neodymium-doped yttrium aluminum garnet (ND: YAG) laser- Bruker, Germany). Data collection time was maintained at 1000 mSec. (co addition 3) for illumination area $50 \times 50\mu m$ diaphragm. Furthermore, fluorescence baseline correction was performed using a third order polynomial, followed by the application of a three-point moving average filter to eliminate most of the perturbing baseline and improve signal to noise ratio.

UV-Vis absorption spectrum of developed RGO was conducted using Jasco V530 spectrometer (Japan). The obtained UV-Vis absorption spectrum was normalized by background and instrument response.
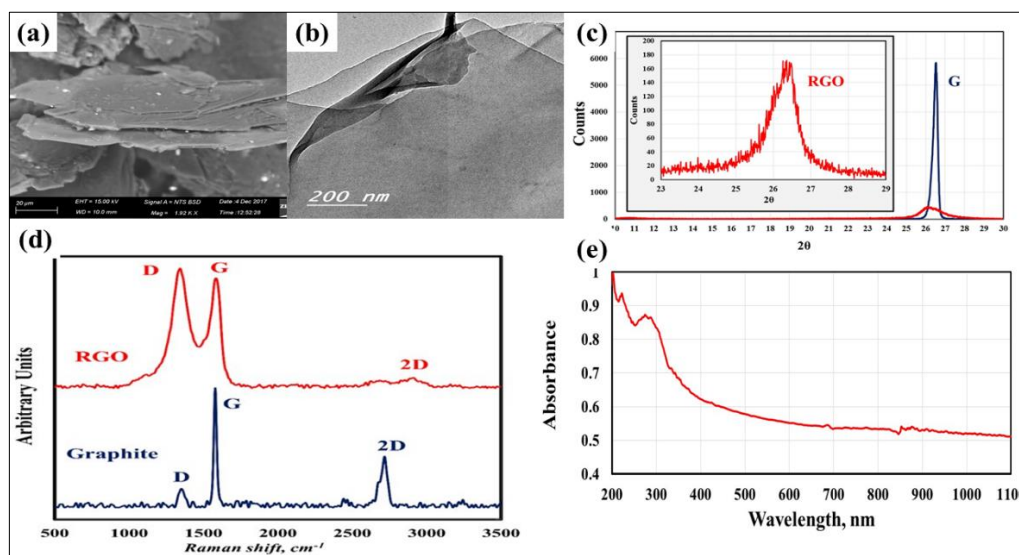

Figure (2): RGO characterization

The graphite precursor was characterized by scanning electron microscopy (SEM). The observed morphological profile of the employed graphite confirmed its flake nature as shown in Figure 2-a. In addition, the SEM micrographs demonstrated multiple-layered structure of 150 μm length. Moreover, TEM micrographs of synthesized RGO demonstrated the successful exfoliation of graphite to RGO. Furthermore, it is obvious that there is no residual reactants or byproducts on RGO surface. The obtained diffraction patterns of the incident beam demonstrated the disappearance of the prominent peak at 20 ~ 26° of graphite precursor in RGO sample as represented in Figure 2-c. The vanishing of the (002) plane of ordered hexagonal graphite structure within RGO confirm the complete successful conversion of graphite to RGO without any detectable graphite impurities.[4, 5]. Figure 2-d represents the acquired Raman spectroscum of developed RGO with respect to starting graphite. Raman spectrum of RGO exhibited G band at $1582\ cm^{-1}$ (typical also for graphite), and broad D band (characteristic for RGO) appears at $1350\ cm^{-1}$; this characteristic peak confirmed the formation of RGO [6-10]. According to the obtained results from TEM, Raman, and

XRD; it is obvious that RGO clearly lost the original graphite structure [8]. Reduction of GO leaves aggregated and randomly packed RGO sheets. The appearance of the (002) with a broad and low intensity XRD peak centered at $2\theta \approx 26.5°$ (d spacing of 3.380 Å) verified successive formation very thin RGO layers due to high degree of exfoliation few layer RGO [4, 5]. The obtained Raman spectra confirm the successive preparation of few-layer reduced graphene oxide with typically thicknesses <10 nm [6, 9, 10]. UV-Vis. absorption spectrum of the synthesized RGO is represented in Figure 2-e.

Recorded RGO absorption at 284 nm could be attributed to $\pi \rightarrow \pi *$ transitions of aromatic C–C bonds [11, 12]. This indicated the formation of highly conjugated structures [13]. low peak observed at 224 nm could be attributed to $n \rightarrow \pi*$ transitions due to any residual oxygenated functional groups [14].preparation for injection by dissolving RGO NANOPARTICLES IN de ionized water then sonication using ultra sound probe ,RGO suspension concentration was 80mg/dl.

Tumour bearing mice:

After obtaining the approval from Cairo University Institutional Animal Care and Use Committee (CU- IACUC) Albino mice weighing about 20-25 grams of the same gender (female), were used for this experiment the animal holding rooms were maintained at constant temperature and humidity on a 12-hour light and dark schedule at an air exchange rate of 18 changes per hour. The animals tested negative for parasitical, bacterial, and viral agents according to the FELASA recommendations. For the surgical procedures, the mice were anesthetized either with a combination of fentanyl/fluanisone and midazolam, or pentobarbital.

A line of Ehrlich ascites Carcinoma (EAC) was supplied from the breading unit of the National Cancer Institute, Cairo University. In this study 1×106 (EAC) cells, single cell suspension were transplanted by subcutaneous inoculation in the mice dorsum using a moderate rate of injection to avoid dispersion flow of the inoculum and to obtain a single grafted tumor ,within seven days after injection the tumors developed and had an average size of ~22 mm^3 .

All tumor developed mice will be divided into four groups 15 mice in each group.

Study groups includes:
The 1st group (G1): will not be subjected to any treatment i.e. considered as sham control group.

The 2nd group (G2): will be subjected to direct intratumoral injection by carbon nanoparticles into the inoculated tumor by a 1cc of water soluble graphine oxide nanoparticles.

The 3th group (G3): will be subjected to near infra-red laser radiation only.

The 4th group (treated group (G4): will be subjected to direct intratumoral injection by graphine oxide nanoparticles into the inoculated tumor by a 1cc of water soluble nanotube carbon nanoparticles then after injection mice.

Photothermal treatment of tumors with RGO:

All mice were irradiated for 5 min at 0.6 w/cm^{2}with a 980 nm NIR laser [G-box medical diode laser systems Giga laser] The laser power was kept constant throughout the irradiation. This led to a rapid temperature rise in the first minute which then levelled to approximately 52–54 °C over the next four minutes. The temperature was monitored continuously by thermal imaging and checked periodically by a thermo probe placed directly in contact with the tumor. The physical appearance of the tumor whitened at the start of irradiation. Thermal images, taken at various time points during the heating, showed that tumors on non-injected mice heated up very slowly and reached an average temperature of 43 °C. In contrast, the tumors of RGO- injected mice reached temperatures of 52.9 °C, thermal imaging indicated that the healthy, illuminated tissue of RGO- injected

mice remained closer to normal body temperature. This confirms that RGO injected tumors were responsible for the absorption of laser light, and subsequent heating of the tumor tissue.

In LASER treatment groups: The mean time to reach treatment temperature at 54 °C during interstitial HPT was 3.2 minutes, NIR lamb time was 4 minutes, control group was 2 minutes; with RGO+LASER time was 1 minute as shown in **figure [3].**
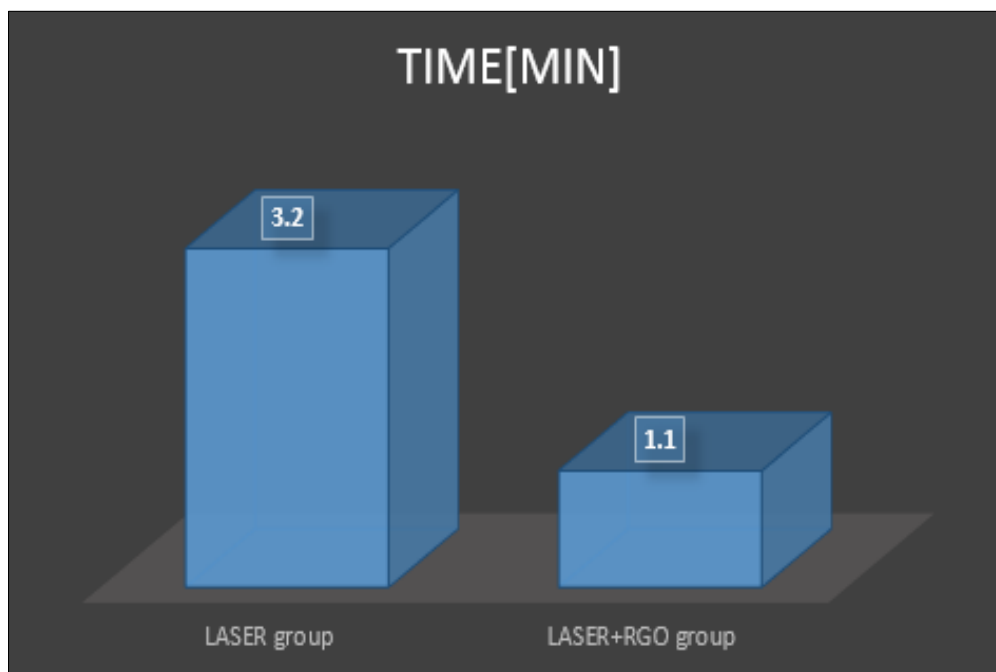

Figure 3: Time required by different methods to reach desired temperature

Measurement of tumor's response to Photothermal treatment with RGO
1-Tumor volume:
After the treatment, tumor diameters were documented three times a week by Vernier caliper measurements in three orthogonal diameters (D_1, D_2, and D_3) where D_1 is the longest diameter, D_2 is the shorter diameter, and D_3 is the height. Tumor volume was calculated by the equation
$$V = (\pi/6)(D_1 \times D_2 \times D_3).$$
These measurements were achieved to all animal groups for 21 days after treatment. The changes in volume of the tumors as affected by different treatment schedules presented as a mean ±SD and shown in tables and graphically represented as growth curves for experimental and control groups.
Tumor growth delay (TGD):
When the tumors were approximately 140 mm^3 in volume as measured by vernier caliper, the treatment was initiated as described before for each group. The

progress of volume for each individual tumor was measured three times a week until it reached a volume of 500mm^3. Tumor growth delay (TGD) was calculated as the additional days taken by each individual treated tumor to reach 500mm^3 beyond that required for untreated controls. (TGD) were calculated as the mean ±SD for the treated group compared to control.
Histopathological Examination:
-Necrosis percent:
Specimens were taken after animal sacrifice by exposure to ether vapor at: 24 hours, 7 days, 14 days and 21days after treatment.
Tumor specimens were excised and fixed in 10% formalin solution, processed by routine paraffin technique; step serial histological sections were prepared from the paraffin blocks and stained with hematoxylin and eosin. Histological picture of the specimens were described.
The specimens taken at, 24 hours and 7days after treatment were subjected to another

semi-quantitative measurement of the necrotic areas that was performed by projecting the microscopic image to a television screen by a video camera attached to the microscope; a translucent paper divided in large number of equal squares was fixed to the television screen. This was repeated in at least five-step section for each paraffin block. So, the necrotic surface area in the microscopic section could be compared to the intact area of the tumor of the same section.

Results
Results of RGO characterization:
The graphite precursor was characterized by scanning electron microscopy (SEM). The observed morphological profile of the employed graphite confirmed its flake nature as shown in Figure 2-a. In addition, the SEM micrographs demonstrated multiple-layered structure of 150 µm length. Moreover, TEM micrographs of synthesized RGO demonstrated the successful exfoliation of graphite to RGO. Furthermore, it is obvious that there is no residual reactants or by-products on RGO surface. The obtained diffraction patterns of the incident beam demonstrated the disappearance of the prominent peak at $2\theta \sim 26°$ of graphite precursor in RGO sample as represented in Figure 2-c. The vanishing of the (002) plane of ordered hexagonal graphite structure within RGO confirm the complete successful conversion of graphite to RGO without any detectable graphite impurities.[4, 5]. Figure 2-d represents the acquired Raman spectroscum of developed RGO with respect to starting graphite. Raman spectrum of RGO exhibited G band at 1582 cm−1 (typical also for graphite), and broad D band (characteristic for RGO) appears at 1350

cm−1; this characteristic peak confirmed the formation of RGO [6-10]. According to the obtained results from TEM, Raman, and XRD; it is obvious that RGO clearly lost the original graphite structure [8]. Reduction of GO leaves aggregated and randomly packed RGO sheets. The appearance of the (002) with a broad and low intensity XRD peak centered at $2\theta \approx 26.5°$ (d spacing of 3.380 Å) verified successive formation very thin RGO layers due to high degree of exfoliation few layer RGO [4, 5]. The obtained Raman spectra confirm the successive preparation of few-layer reduced graphene oxide with typically thicknesses <10 nm [6, 9, 10]. UV-Vis. absorption spectrum of the synthesized RGO is represented in Figure 2-e. Recorded RGO absorption at 284 nm could be attributed to $\pi \rightarrow \pi *$ transitions of aromatic C–C bonds [11, 12]. This indicated the formation of highly conjugated structures [13]. low peak observed at 224 nm could be attributed to $n \rightarrow \pi*$ transitions due to any residual oxygenated functional groups [14].

Tumour size changes:
Control Group
Before treatment had started the tumors from all groups was ellipsoid in shape with regular contour, more or less flattened under surface and firm consistence. The overlaying skin presented neither special adhesions nor abnormal vascularity.

The Ehrlich carcinoma tumor cells transplanted subcutaneously in the mice and reached a volume range of 119.8-130.5mm3, within 7-8 days after transplantation (the day of starting treatment in the other groups). Tumors continued to grow and reached a volume range of 1.260-1.504 mm3 after 21 days the tumor was a cauliflowe like at that time with no special skin signs.
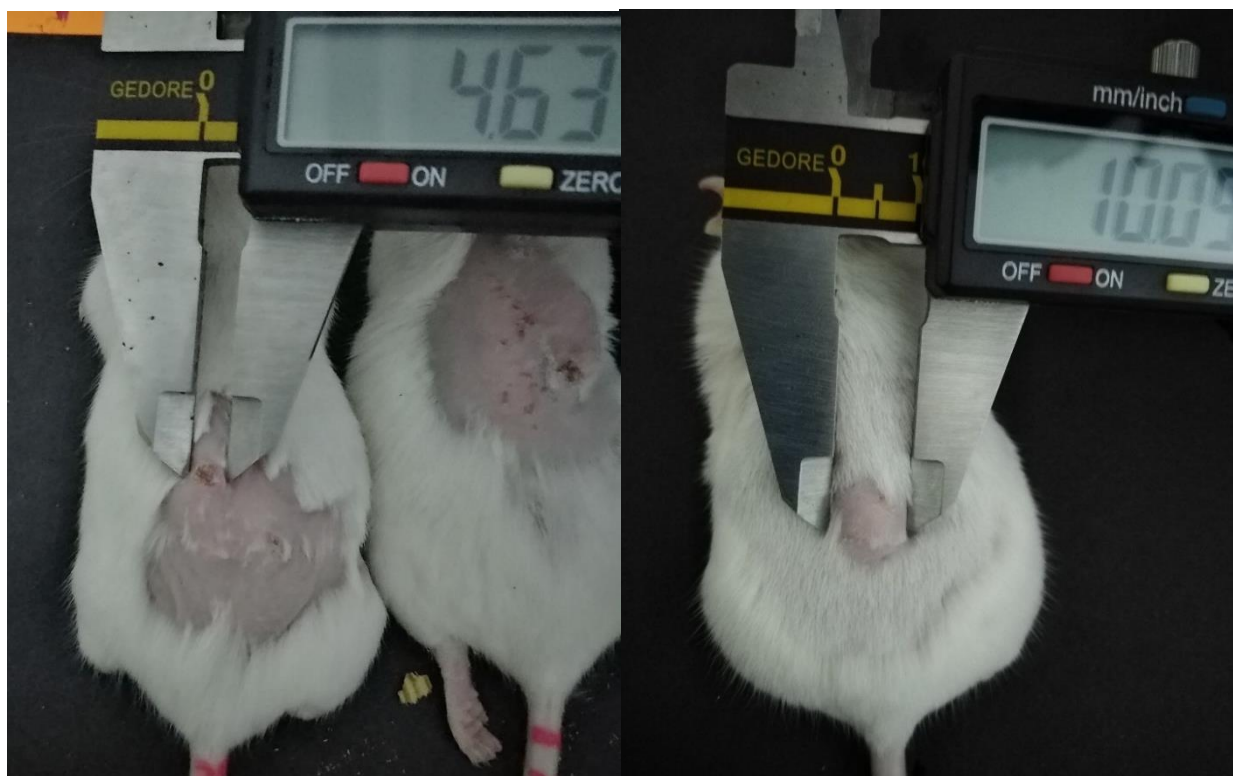
Eur. Chem. Bull. **2023**, *12(Special Issue 9)*, 2644-2656

2650

Figure4a Shows the difference in tumor size between the control group at the beginning of treatment (right) and 21 days later (left)

Figure4b after treatment with combined LASER&RGO

Tumor growth delay results (TGD):
The untreated control group needed 13 days to reach a mean tumor volume about 500 ± 8.2 mm^3. The extra days needed by the other treatment groups to reach this volume known as tumor growth delay (TGD) and were presented as mean (±SD) as following Table

Table 3. showing tumor growth delay in days in each treatment group.

Treatment Groups	TUMOR GROWTH DELAY [days]
RGO group[G2]	1.35
LASER hyperthermia group[G3]	2.7
LASER+RGO group[G4]	15.6
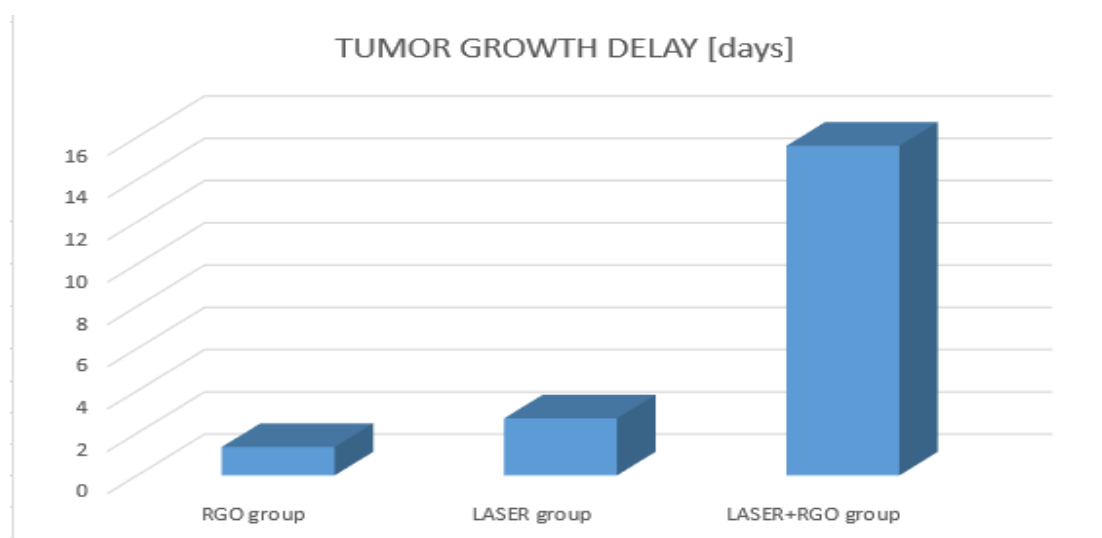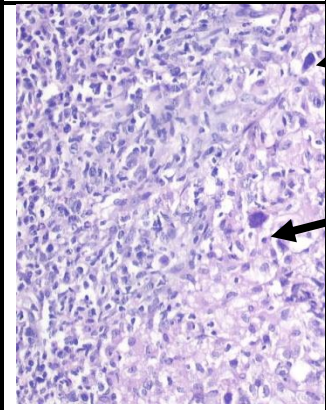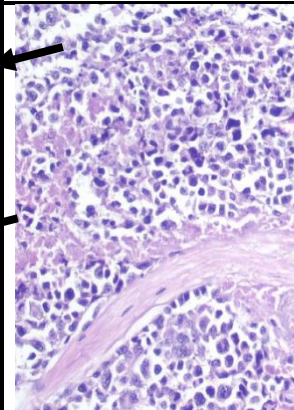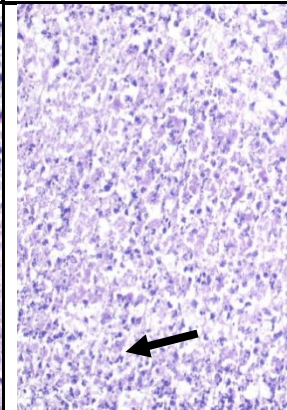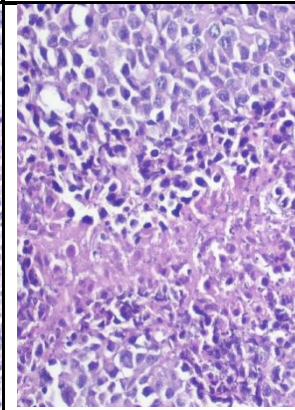
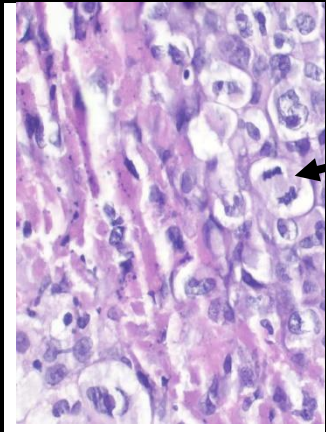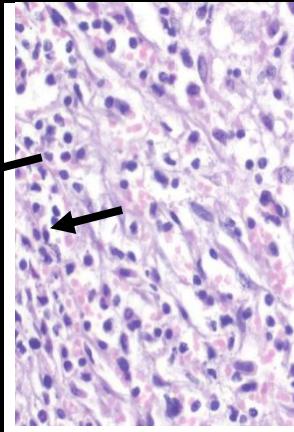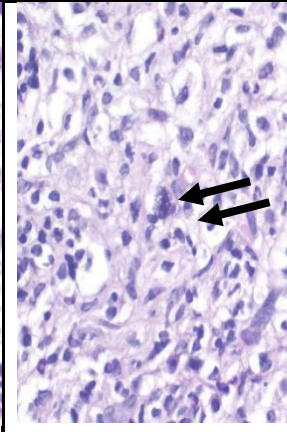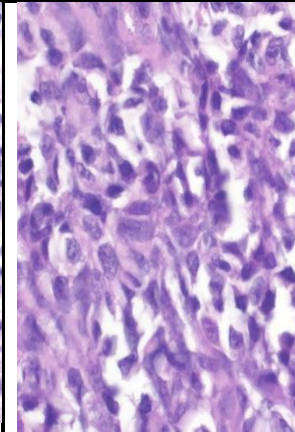**Fig 5.** showing tumor growth delay in days

Pathological results:
The extension of necrotic area and mitotic index were assessed as previously described (Gardouh et al. 2018)[15]. The necrotic area was evaluated using the ImageJ 1.45F (NIH, USA) and the mean was calculated for each group. The mitotic figures were counted in 10 consecutive high-power fields (X40) for each section and the mean was calculated for each group so microscopic examination of G1 group showed aggressive neoplastic cells that arranged in solid sheets with severe anisocytosis and anisokaryosis. The nuclei appeared hyperchromatic, with pleomorphism, numerous mitotic figures, frequent bizarre mitosis and several tumor giant cells. Necrosis was less detected in the examined tumor masses associated with invasion of the surrounding muscles bundles with subsequent necrosis of the muscle fibres (**Fig. 5-6**). Similar results were recorded in G2, G3 and G4 groups, however marked reduction of the number of infiltrating neoplastic cells in these groups accompanied by increase necrotic areas with intense mononuclear inflammatory cells infiltration (**Fig. 7-12**). Higher improvement was noticed in G5 group with marked reduction of mitotic number and increase necrotic areas (**Fig. 13-14**).

The statistical analysis of necrosis area % showed a significant decrease in the area % in G1 and G2 compared to other groups. Absence of significance was recorded between G3 and G4 groups. Concerning mitotic figure, G1 group showed a significant increase when compared to other groups. No significant difference was detected between G2, G3 and G4 groups.

| G1 group	G2group	G3 group	G4
Fig. (5) Photomicrograph of solid tumor, G1 group Showing solid aggregation of neoplastic cells with marked anisocytosis, anisokaryosis and hyperchromatic nuclei (arrows) (H&E).	**Fig. (9)** Photomicrograph of solid tumor, G2 group showing variable number of neoplastic cells with increase necrotic area (arrow) (H&E).	**Fig. (13)** Photomicrograph of solid tumor, G3 group showing diffuse necrosis of the neoplastic cells (H&E).	**Fig. (11)** Photomicrograph of solid tumor, G4 group showing solid aggregation of neoplastic cells with moderate necrotic areas (arrow) (H&E).
Fig. (6) Photomicrograph of solid tumor, G1 group showing numerous mitosis among the neoplastic cells (arrows) (H&E).	**Fig. (11)** Photomicrograph of solid tumor, G2 group showing reduction number of neoplastic cells with existence of giant cell (arrow) (H&E).	**Fig. (14)** Photomicrograph of solid tumor, G3 group showing marked decrease number of neoplastic cells (arrow) with variable number of mononuclear cells (H&E).	**Fig. (8)** Photomicrograph of solid tumor, G4 group showing solid aggregation of neoplastic cells with moderate anisocytosis and anisokaryosis (H&E).
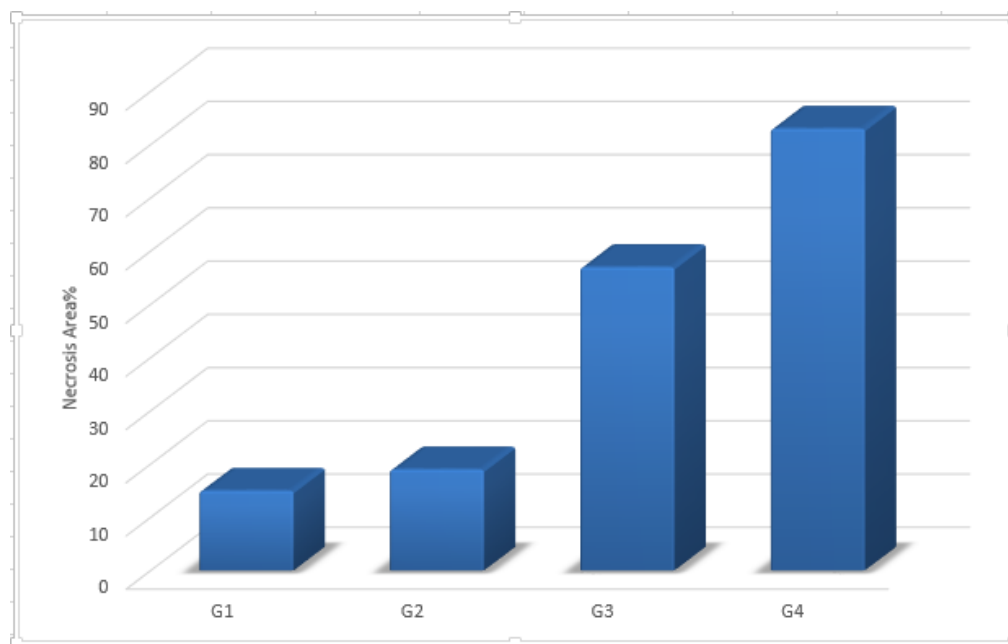
Fig. 15: Chart illustrating the necrosis area %in different groups. Values expressed as means ± SE. Significant difference was considered at *p< 0.05*. Significant from G1, significant from G2, significant from G3, & significant from G4, β significant from G5.

Fig. 16: Chart illustrating mitotic index in different groups. Values expressed as means ± SE. Significant difference was considered at *p< 0.05*. Significant from G1, significant from G2, significant from G3, & significant from G4, β significant from G5.
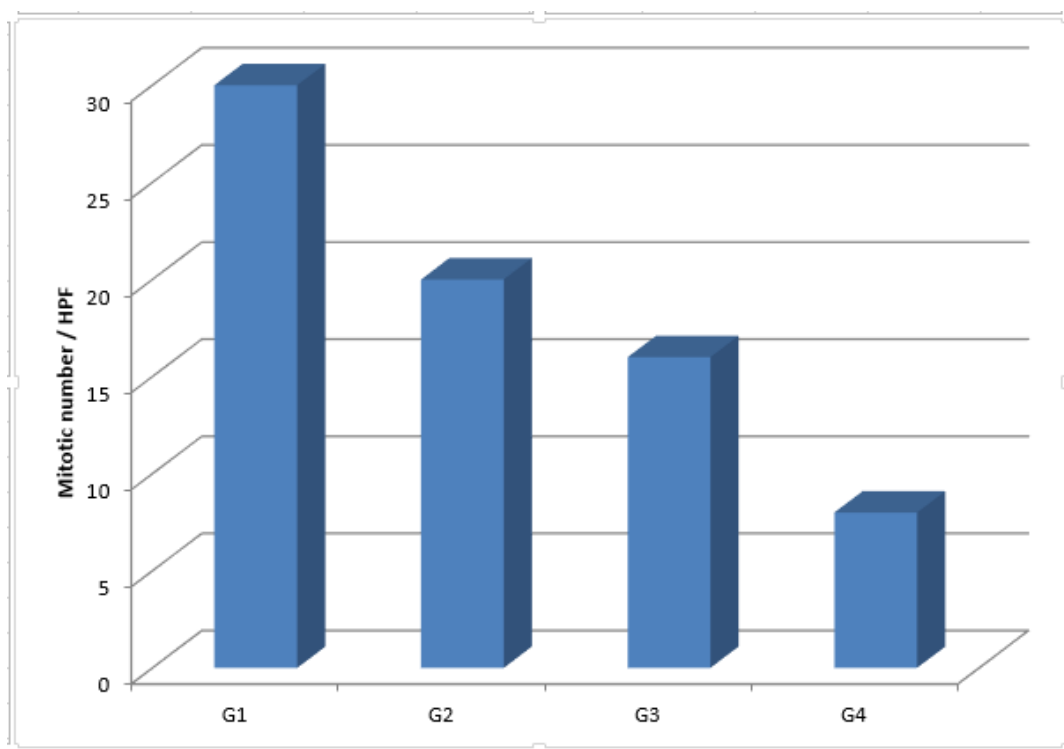
Results Histopathological tumour cell destruction assessment:

The necrotic surface area was compared to the non-necrotic tumor surface area and expressed as the necrosis present. This necrosis percent reflects approximately the effeteness of treatment modality. It was calculated in each specimen in all the treatment groups one and 7 days after treatment.

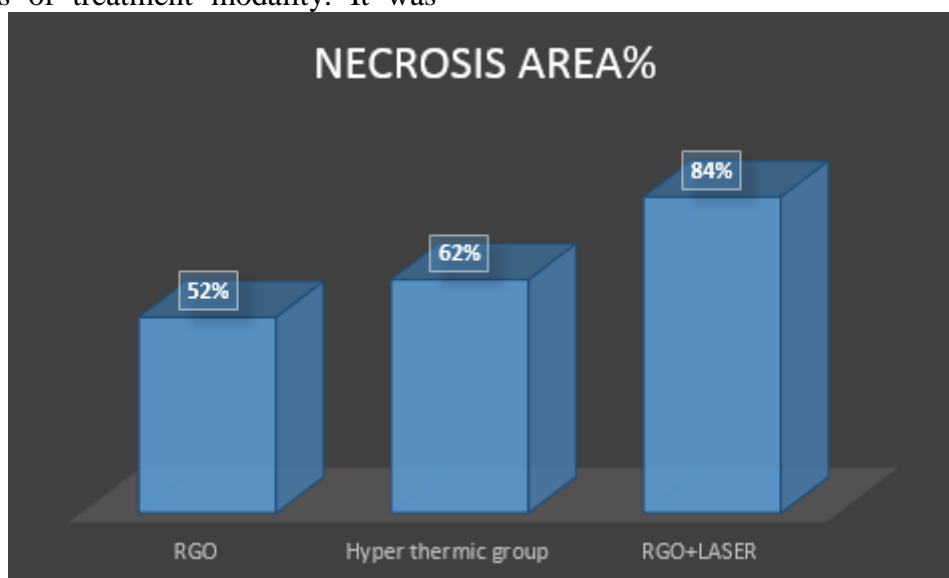The results of necrosis percent after microscopic examination of the specimens as shown in the graph below

Fig 18 showing necrosis area in each group

♦ *In HPT treatment groups*: Surface HPT at 42°C showed necrosis percent of 30.1 ± 0.2 % one day after which increased significantly ($P<0.05$) to $52.4 \pm 25\%$ after 7 days of starting treatment.

♦ *The combined RGO&NIR group* showed necrosis percent $41.8 \pm 1.3\%$ one day after treatment that was significantly ($P<0.05$) less than the necrosis percent of $62.1 \pm 4.7\%$ occurred 7 days after treatment.

One week after treatment the mean necrosis percent produced by the combined treatment group was significantly more than the necrosis percent produced by the group treated with *HPT*

♦ *The combined RGO&LASER group* showed necrosis percent $41.8 \pm 1.3\%$ one day after treatment that was significantly ($P<0.05$) less than the necrosis percent of $84 \pm 4.7\%$ occurred 7 days after treatment.

One week after treatment the mean necrosis percent produced by the combined treatment group was significantly more than the necrosis percent produced by both the previous groups.

Conclusions:

The concept of pre-conditioning the tumor microenvironment using nanoparticles is relatively new and many researches particularly for photo thermal therapy remain largely open so our group has demonstrated that chemical preparation of reduced RGO then its usage in photothermal treatment of malignant tumor and standing on advantage, disadvantage for this method of treatment reavling successful preparation of reduced RGO and successful treatment of locally malignant tumor combined with photothermal treatment using diode laser as described before in result. also more soluble carbon nanoparticle are needed for systemic use as constantly evolving and heterogeneous nature of cancer and its metastasis.

REFERENCES

[1] N.I. Zaaba, K.L. Foo, U. Hashim, S.J. Tan, W.W. Liu, C.H. Voon, Synthesis of Graphene Oxide using Modified Hummers Method: Solvent Influence, Procedia Engineering 184 (2017) 469-477.

[2] S.N. Alam, N. Sharma, L. Kumar, Synthesis of graphene oxide (GO) by modified hummers method and its thermal reduction to obtain reduced graphene oxide (rGO), J Graphen 6(1) (2017) 1-18.

[3] M.J. Yoo, H.B. Park, Effect of hydrogen peroxide on properties of graphene oxide in Hummers method, Carbon 141 (2019) 515-522.

[4] S. Abdolhosseinzadeh, H. Asgharzadeh, H.S. Kim, Fast and fully-scalable synthesis of reduced graphene oxide, Scientific reports 5 (2015) 10160.

[5] A. Shalaby, D. Nihtianova, P. Markov, A. Staneva, R. Iordanova, Y. Dimitriev, Structural analysis of reduced graphene oxide by transmission electron microscopy, Bulg. Chem. Commun 47(1) (2015) 291-295.

[6] D.C. Marcano, D.V. Kosynkin, J.M. Berlin, A. Sinitskii, Z. Sun, A. Slesarev, L.B. Alemany, W. Lu, J.M. Tour, Improved synthesis of graphene oxide, ACS nano 4(8) (2010) 4806-4814.

[7] Z. Ni, Y. Wang, T. Yu, Z. Shen, Raman spectroscopy and imaging of graphene, Nano Research 1(4) (2008) 273-291.

[8] M. Sarno, A. Senatore, C. Cirillo, V. Petrone, P. Ciambelli, Oil lubricant tribological behaviour improvement through dispersion of few layer graphene oxide, Journal of nanoscience and nanotechnology 14(7) (2014) 4960-4968.

[9] J.H. Warner, F. Schaffel, M. Rummeli, A. Bachmatiuk, Graphene: fundamentals and emergent applications, Newnes2012.

[10] H. Zhang, P.X. Feng, Fabrication and characterization of few-layer graphene, Carbon 48(2) (2010) 359-364.

[11] J. Zhang, H. Yang, G. Shen, P. Cheng, J. Zhang, S. Guo, Reduction of graphene oxide via L-ascorbic acid, Chemical Communications 46(7) (2010) 1112-1114.

[12] D. Luo, G. Zhang, J. Liu, X. Sun, Evaluation criteria for reduced graphene oxide, The Journal of Physical Chemistry C 115(23) (2011) 11327-11335.

[13] Y.H. Ding, P. Zhang, Q. Zhuo, H.M. Ren, Z.M. Yang, Y. Jiang, A green approach to the synthesis of reduced graphene oxide nanosheets under UV irradiation, Nanotechnology 22(21) (2011) 215601.

[14] V.H. Pham, H.D. Pham, T.T. Dang, S.H. Hur, E.J. Kim, B.S. Kong, S. Kim, J.S. Chung, Chemical reduction of an aqueous suspension of graphene oxide by nascent hydrogen, Journal of Materials Chemistry 22(21) (2012) 10530-10536.

[15] Gardouh, Ahmed R., Bassant M. Barakat, Mona K. E. Qushawy, Amany Y. El-kazzaz, Manal M. Sami, and Sawsan A. Zaitone. 2018. "Antitumor Activity of a Molecularly Imprinted Nanopreparation of 5-Flurouracil against Ehrlich's Carcinoma Solid Tumors Grown in Mice: Comparison to Free 5-Flurouracil." *Chemico-Biological Interactions* 295(March):52–63.